COMPOSITE ELECTRODES FOR LITHIUM BATTERIES

by

M. M. Thackeray, K. D. Kepler, J. T. Vaughey, A. J. Kahaian,, C. S. Johnson
Electrochemical Technology Program
Chemical Technology Division
Argonne National Laboratory
Argonne, IL U.S.A.

and

Y. Shao-Horn, and S. A. Hackney
Department of Metallurgical and Materials Engineering
Michigan Technological University,
Houghton, Michigan, U.S.A.

September 22, 1998

To be presented at the 12th IBA Battery Materials Symposium, Grenoble-Annecy, Imperial Palace, Annecy, France, September 27-October 2, 1998

DISCLAIMER

DISCLAIMER

Portions of this document may be illegible in electronic image products. Images are produced from the best available original document.

Composite Electrodes for Lithium Batteries

M. M. Thackeray, C. S. Johnson, A. J. Kahaian, K. D. Kepler and J. T. Vaughey
Chemical Technology Division, Argonne National Laboratory,
Argonne, Illinois 60439, USA
and
Y. Shao-Horn and S. A. Hackney
Department of Metallurgical and Materials Engineering
Michigan Technological University, Houghton, Michigan 49931, USA

Abstract

The stability of composite positive and negative electrodes for rechargeable lithium batteries is discussed. Positive electrodes with spinel-type structures that are derived from orthorhombic-$LiMnO_2$ and layered-MnO_2 are significantly more stable than standard spinel $Li[Mn_2]O_4$ electrodes when cycled electrochemically over both the 4-V and 3-V plateaus in lithium cells. Transmission electron microscope data of cycled electrodes have indicated that a composite domain structure accounts for this greater electrochemical stability. The performance of composite Cu_xSn materials as alternative negative electrodes to amorphous SnO_x electrodes for lithium-ion batteries is discussed in terms of the importance of the concentration of the electrochemically inactive copper component in the electrode.

Introduction

The lithium-manganese-oxide spinel, $LiMn_2O_4$, and slightly modified compositions $Li_{1+\delta}Mn_{2-\delta}O_4$ ($0<\delta<0.05$) are of interest as positive electrodes for lithium-ion batteries [1-3]. The useful rechargeable capacity of a $Li_xMn_2O_4$ spinel electrode for 4-V cells is limited to the compositional range $0<x\leq 1$, over which the cubic symmetry of the spinel structure is maintained. For the range $1<x<2$, the electrode provides 3 V vs. lithium. Severe capacity loss is observed on cycling the spinel electrode at 3 V because of a change in crystal symmetry from cubic to tetragonal [1]. Thus, although the theoretical capacity of the spinel electrode over the 4-V and 3-V plateaus is an attractive 308 mAh/g (based on the mass of the $[Mn_2]O_4$ spinel framework), only approximately half of this is accessible in 4-V lithium-ion cells. By contrast, orthorhombic-$LiMnO_2$ and

layered-$LiMnO_2$ electrodes transform to spinel structures on electrochemical cycling and provide significantly superior stability to standard $LiMn_2O_4$ electrodes when cycled over both the 4-V and 3-V plateaus [4-7]. The first part of this paper presents microstructural information about electrodes derived from orthorhombic-$LiMnO_2$ and layered-$LiMnO_2$ and offers an explanation for their enhanced electrochemical stability.

Intermetallic compounds based on copper-tin [8] and iron-tin [9] have recently been investigated as alternative materials to amorphous tin oxide (SnO_x) negative electrodes for lithium-ion cells recently reported by Fujifilm Celtec [10]. The advantage of using a copper-tin electrode is that the copper component of the composite electrode is an inert metal at low voltages vs. lithium with excellent electronic conductivity and, therefore, can act as a current collector. Furthermore, copper does not combine with lithium to any significant extent, thus offering a solution to the irreversible capacity loss associated with Li_2O formation during charge of SnO_x electrodes [11]. The significant improvement in electrochemical behavior, particularly with respect to cycle life, that can be obtained from small-grained composite structures such as $SnSb_x$ and $SnAg_x$ ($x \leq 0.3$) has already been comprehensively studied by Besenhard and co-workers [12].

The second part of the paper discusses the stability and electrochemical behavior of composite $Cu_6Sn_{5\pm\delta}$ electrodes, particularly those derived from the intermetallic eta-phase, Cu_6Sn_5, that contains a large amount of electrochemically "inactive" copper in the structure. An analogy is drawn to insertion electrode materials, such as MnO_2, V_2O_5 and LiV_3O_8 in which the transition metal ions can be considered as the electrochemically active component and oxygen ions as the inactive component.

Experimental

Orthorhombic-$LiMnO_2$ [13], layered-MnO_2 [14] and $Cu_6Sn_{5\pm\delta}$ [8] electrode materials were prepared by methods similar to those reported in the references. Details of coin cell (size 1225) fabrication and electrochemical evaluation are provided in reference 15. Microscopic images of the parent and cycled electrodes were obtained on a JEOL-JSM 6400 scanning electron microscope and a JEOL-JEM 40001FX-1 high-resolution transmission electron microscope.

Results and Discussion

Electrochemistry of $LiMn_2O_4$, Orthorhombic-$LiMnO_2$ and Layered-$LiMnO_2$ Electrodes

The typical electrochemical profiles of lithium cells with $LiMn_2O_4$, orthorhombic-$LiMnO_2$ and layered-$LiMnO_2$ electrodes are shown in Fig. 1. Cells with $LiMn_2O_4$ and orthorhombic-$LiMnO_2$ electrodes (Fig. 1a, b) were cycled ten times between 4.5 and 2.0 V [4]. The cell with a layered-$LiMnO_2$ electrode was cycled sixty times between 4.7 and 2.3 V [7]. After the first cycle, it is clear from the figures that the cells with orthorhombic-$LiMnO_2$ and layered-$LiMnO_2$ electrodes adopt strong spinel-like behavior with characteristic plateaus at approximately 4 V and 3 V; the plateau at 4 V is attributed to the insertion (extraction) of lithium into (from) tetrahedral sites, and the plateau at 3 V to the insertion (extraction) of lithium into (from) octahedral sites [1, 16]. There is a striking difference in the cycling stability of the cells. The rapid decline in capacity of cells with the standard spinel electrode (Fig. 1a), particularly at 3 V, is attributed to a structural instability of $Li_xMn_2O_4$ compared to the stability of the spinel-like electrodes derived electrochemically from orthorhombic-$LiMnO_2$ and layered-$LiMnO_2$.

Transmission Electron Microscopy of Cycled $LiMn_2O_4$, Orthorhombic-$LiMnO_2$ and Layered-$LiMnO_2$ Electrodes

Convergent beam electron diffraction patterns (001 zone axis projections) of cycled $Li_xMn_2O_4$ electrodes are shown in Fig. 2. Figure 2a represents the typical pattern of cubic (4 V) $Li_xMn_2O_4$ electrodes ($0<x\leq 1$) having some lithium in the tetrahedral sites, as indicated by the presence of the relatively weak (022) diffraction spots. Figure 2c is the pattern of a fully lithiated spinel structure with tetragonal symmetry ($c/a\approx 1.16$) observed in electrodes at 3 V. The absence of the (022) diffraction spots in Fig. 2c is confirmation of the ordered rock-salt configuration $Li_2[Mn_2]O_4$ (where the square brackets represent the 16d octahedral sites of the spinel structure with symmetry Fd3m). Figure 2b represents the pattern of a crystallite, observed typically at the surface of lithiated $Li_{1+x}Mn_2O_4$ spinel particles; it shows the tetragonal phase emanating from the cubic $LiMn_2O_4$ structure. The mismatch between the cubic and the tetragonal phases results in a nearly five-degree rotation of the two unit cells and represents a fracture at the

phase boundary. This fracture causes a loss of particle to particle contact which is believed to be largely responsible for the capacity fade observed in 3-V $Li/LiMn_2O_4$ cells.

Cycled electrodes derived from orthorhombic-$LiMnO_2$ exhibit the same structural trend as that observed with standard $LiMn_2O_4$ spinel electrodes. The electron diffraction pattern of the parent orthorhombic-$LiMnO_2$ (001 zone axis projection) is shown in Fig. 3a. The electron diffraction patterns of electrodes that had been extracted from the cell after a charge onto the 4-V plateau and after discharge onto the 3-V plateau showed crystallites with the characteristic cubic and tetragonal symmetries of spinel and rocksalt phases, respectively, similar to those shown in Fig. 2a and 2c. In addition, cells that had only been cycled a few times showed evidence of the transition of the orthorhombic-$LiMnO_2$ structure to spinel (Fig. 3b). In this case, the good alignment of the two unit cells along a single zone axis provides evidence that there is a strong compatibility between the oxygen array of the parent compound and the oxygen array of the lithiated spinel, consistent with the mechanism provided for the orthorhombic-$LiMnO_2$ to spinel transformation [17].

Similar observations have been made in the electrochemical conversion of layered $LiMnO_2$ electrodes to spinel [7]; the electron diffraction data of cycled electrodes have shown patterns typical of a cubic spinel and a tetragonal spinel, as well as "intermediate" patterns representative of a layered-type structure intergrown with a spinel-type structure. The question that arises is why do the electrochemically prepared structures provide greater stability to electrochemical cycling than chemically prepared $LiMn_2O_4$ electrodes? Clues to this behavior are found in the transmission electron micrograph images of cycled orthorhombic-$LiMnO_2$ and layered-$LiMnO_2$ electrode structures in Fig. 4a and 4b, respectively. Both images, which are characterized by non-uniform electron diffraction contrasts, show structures that are composed predominantly of microdomains of spinel in an intergrown composite matrix. These features provide very strong evidence that the conversion to spinel does not occur in a systematic and uniform process, and that the migration of manganese on extraction of lithium from both orthorhombic-$LiMnO_2$ and layered-$LiMnO_2$ structures does not result in the ideal $[Mn_2]O_4$ spinel framework. This non-ideal behavior can be readily understood if during the transformation some lithium

ions are locked in sites corresponding to the octahedral 16d sites of the spinel structure. Such a process would result in discrete $[Mn_{2-\delta}Li_{\delta}]_{16d}O_4$ spinel domains ($0<\delta<0.33$) (and/or enantiomeric $[Mn_{2-\delta}Li_{\delta}]_{16c}O_4$ domains [18]) of varying composition and lattice parameter, which are known to be more stable to electrochemical cycling at 3 V compared to the standard $[Mn_2]O_4$ spinel framework [3]. Evidence of a structure with spinel domains embedded and intergrown within a residual Li_xMnO_2 framework ($x<1$) has already been reported for electrodes derived from layered-$LiMnO_2$ [7]. It is believed that the composite nature of the electrode resulting from the presence of the $[Mn_{2-\delta}Li_{\delta}]O_4$ spinel domains (with δ slightly greater than zero) may, therefore, contribute to the enhanced stability of these electrodes to electrochemical cycling at 3 V.

Intermetallic Copper-Tin Composite Electrodes

The concept of using copper-tin composite electrodes derived from intermetallic phases such as Cu_6Sn_5 and Li_2CuSn was recently reported [8]. Cu_6Sn_5 has a layered structure, in which, in the ideal configuration, the copper atoms have octahedral coordination and the tin atoms have trigonal prismatic coordination [8]. There is no significant interstitial space within the structure to accommodate additional lithium. The reaction of lithium with Cu_6Sn_5 thus takes place via a displacement reaction, during which it is expected that lithium alloys with the tin component to form a series of Li_xSn compounds within a Li_xSn/Cu composite matrix. A schematic illustration of the reaction from a crystalline Cu_6Sn_5 structure to a Li_xSn/Cu composite matrix is shown in Fig. 5.

This reaction can be considered, on a macroscopic scale, to be analogous to the insertion of lithium into a host electrode structure such as MnO_2. Provided that the copper-tin particles are sufficiently small and the composite electrode maintains sufficient porosity to allow access of lithium to the tin grains and to cater for volume expansion, such copper-tin electrodes should provide superior stability to electrochemical cycling compared to pure Li_xSn alloy electrodes. The structural rigidity of inactive components in alloy systems and the importance of grain size and microstructure have already been stressed in many papers by Huggins and Besenhard [12, 19-23]. The analogy to insertion compounds such as MnO_2, V_2O_5 and LiV_3O_8 in which the ratio of inactive:active

components is 2:1, 2.5:1 and 2.67:1, respectively, suggests that the amount of inactive component required to stabilize alloy systems may be much higher than previously explored. For example, electrodes formed by electrochemically co-depositing Sn and Sb (in which Sn is considered inactive at the potentials at which Sb is active), or Sn and Ag, have typically had inactive:active ratios of 0.3:1 or less [12].

Scanning Electron Microscope Images of Cu_6Sn_5

Scanning electron microscope images of a typical Cu_6Sn_5 electrode, prepared first by reacting copper and tin powders under an inert atmosphere at 400°C, followed by milling are shown in Fig. 6. The images of the microstructure and element mapping by energy dispersive analysis of X-rays (using the L-lines of Sn and Cu) indicate that the powder has an average particle size of approximately 1 μm and a very uniform distribution of copper and tin within the grains.

Electrochemistry of $Cu_6Sn_{5+\delta}$ Electrodes (δ=-1, 0, 1)

Figure 7a presents a typical "discharge and charge" curve of a Li/Cu_6Sn_5 cell that represents the insertion and extraction of lithium from a copper-tin composite electrode when cycled between 1.2 and 0 V. Apart from the initial reaction that occurs on the second discharge at approximately 400 mV vs. lithium, the absence of discrete plateaus that would normally be associated with the electrochemical formation of individual Li_xSn phases has been attributed to the Li_xSn and Cu grain sizes and to the microstructural and morphological features of the composite electrode [8]. When cycled between 1.2 and 0 V, the Cu_6Sn_5 electrode delivers an attractive 400 mAh/g; with a density of 8.28 g/ml, this translates to a volumetric capacity of 3312 mAh/ml. However, Cu_6Sn_5 electrodes that are deeply "discharged" lose capacity steadily [8]. Raising the cutoff voltage from 0 to 0.2 V yields a significant improvement in capacity retention, but at the expense of capacity; preliminary data show that a steady capacity of approximately 200 mAh/g (1656 mAh/ml) can be achieved during the first twenty cycles (Fig. 7b). Of particular significance is that the largest capacity and greatest stability is achieved when the concentration of copper in the composite $Cu_6Sn_{5+\delta}$ electrode is highest (Cu_6Sn_4).

Conclusions

This study has demonstrated that composite structures can greatly enhance the capacity and cycling stability of metal oxide insertion electrodes such as the spinel $Li_{1+x}Mn_2O_4$ and alloy systems such as Li_xSn which undergo large volume changes during reaction with lithium. The enhanced stability of positive spinel electrodes that are derived electrochemically from orthorhombic- or layered-$LiMnO_2$ structures can be attributed to domains of intergrown spinel phases of varying composition in the $Li_{1+\delta}Mn_{2-\delta}O_4$ spinel system ($0<\delta<0.33$) embedded within a matrix derived from the parent electrodes. Lithium-tin alloy systems that are of interest as negative electrode materials and that operate predominantly by displacement reactions can be stabilized on a macroscopic level by discrete grains of an electronically conducting "inactive" matrix, such as copper. The concentration of the inactive component plays an important role in controlling the electrochemical behavior of the composite electrode.

Acknowledgments

Support from the U.S. Department of Energy Advanced Battery Program, Chemical Sciences Division, Office of Basic Energy Sciences under contract W-31-109-ENG-38 is gratefully acknowledged.

References

1. M. M. Thackeray, *Prog. Solid State Chem.*, **25**, 1 (1997).
2. J. M. Tarascon, E. Wang, F. K. Shokoohi, W. R. McKinnon and S. Colson, *J. Electrochem. Soc.*, **138**, 2859 (1991).
3. R. J Gummow, A. de Kock and M. M. Thackeray, *Solid State Ionics*, **69**, 59-67 (1994).
4. R. J. Gummow and M. M. Thackeray, *J. Electrochem. Soc.*, **141**, 1178-1182 (1994).
5. I. Koetschau, M. N. Richard, J. R. Dahn, J. B. Soupart and J. C. Rousche, *J. Electrochem. Soc.*, **142**, 2906-2910 (1995).
6. Y.-I. Jang, B. Huang, H. Wang, D.R. Sadoway, and Y.-M. Chiang, Ext. Abstr. 132, 194th Meeting of the Electrochem. Soc., Boston (Nov. 1-6) 1998.
7. Y. Shao-Horn, S. A. Hackney, A. R. Armstrong, P. G. Bruce, R. Gitzendanner, C. S. Johnson and M. M. Thackeray, *J. Electrochem. Soc.* (1998). In press.
8. J. T. Vaughey, K. D. Kepler, D. R. Vissers and M. M. Thackeray, a) Ext. Abstr. (Tues 82), 9th Int. Meeting on Lithium Batteries, Edinburgh, Scotland (July 12-17) 1998, b) *Journal of Power Sources* (1998). Submitted.
9. O. Mao, R. A. Dunlap and J. R. Dahn, a) Ext. Abstr. (Tues 32-34), 9th Int. Meeting on Lithium Batteries, Edinburgh, Scotland (July 12-17) 1998, b) *Journal of Power Sources* (1998). Submitted.
10. Y. Idota, T. Kubota, A. Matsufuji, Y. Maekawa, and T. Miyasaka, *Science*, **276**, 1395 (1997).
11. I. A. Courtney and J. R. Dahn, *J. Electrochem. Soc.*, **144**, 2045 (1997).
12. J. O. Besenhard, J. Yang, and M. Winter, *J. Power Sources*, **68**, 87 (1997).
13. I. J. Davidson, R. S. McMillan, J. J. Murray and J. E. Greedan, *J. Power Sources*, **54**, 232-235 (1995).
14. A. R. Armstrong and P. G. Bruce, *Nature*, **381**, 499 (1996).
15. C. S. Johnson, D. W. Dees, M. F. Mansuetto, M. M. Thackeray, D. R. Vissers, D. Argyriou, C.-K. Loong, and L. Christensen, *J. Power Sources*, **68**, 570 (1997).
16. J. B. Goodenough, M. M. Thackeray, W. I. F. David and P. G. Bruce, *Rev. de Chim. Min.*, **23**, 435-455 (1984).
17. R. J. Gummow, D. C. Liles and M. M. Thackeray, *Mat. Res. Bull.*, **28**, 1249 (1998).
18. M. M. Thackeray, *J. Electrochem. Soc.*, **144**, L100 (1997).
19. J. Wang, I. D. Raistrick, and R. A. Huggins, *J. Electrochem. Soc.*, **133**, 457 (1986).
20. J. O. Besenhard, P. Komenda, A. Paxinos, E. Wudy, and M. Josowicz, *Solid State Ionics*, **18-19**, 823 (1986).
21. B. A. Boukamp, G. C. Lesh and R. A. Huggins, *J. Electrochem. Soc.*, **128**, 725 (1981).
22. J. O. Besenhard, M. Hess and P. Komenda, *Solid State Ionics*, **40-41**, 525 (1990).
23. J. Yang, M. Winter and J. O. Besenhard, *Solid State Ionics*, **90**, 281 (1996).

Captions to Figures

Fig. 1. Electrochemical profiles of a) $LiMn_2O_4$ [4], b) orthorhombic-$LiMnO_2$ [4] and c) layered-$LiMnO_2$ [7] electrodes in lithium cells.

Fig. 2. Electron diffraction patterns of a) $LiMn_2O_4$ (cubic), b) $LiMn_2O_4$ (cubic) and $Li_2Mn_2O_4$ (tetragonal), and c) $Li_2Mn_2O_4$ (tetragonal). ([001] zone axes).

Fig. 3. Electron diffraction patterns of a) parent orthorhombic-$LiMnO_2$ and b) a cycled orthorhombic-$LiMnO_2$ electrode.

Fig. 4. Transmission electron microscope images of a) cycled orthorhombic-$LiMnO_2$ and b) cycled layered-$LiMnO_2$ electrodes, showing microdomains of spinel in (composite) microstructures.

Fig. 5. A schematic representation of the reaction of crystalline Cu_6Sn_5 with lithium leading to a composite matrix containing domains of metallic Cu and lithiated tin (Li_xSn).

Fig. 6. Scanning electron microscope images and element mapping of a Cu_6Sn_5 electrode powder.

Fig. 7. a) Typical voltage profile of a Li/Cu_6Sn_5 cell (voltage range 1.2 to 0 V), and b) capacity vs. cycle number plot for Li/$Cu_6Sn_{5+\delta}$ cells (voltage range: 1.2 to 0.2 V).

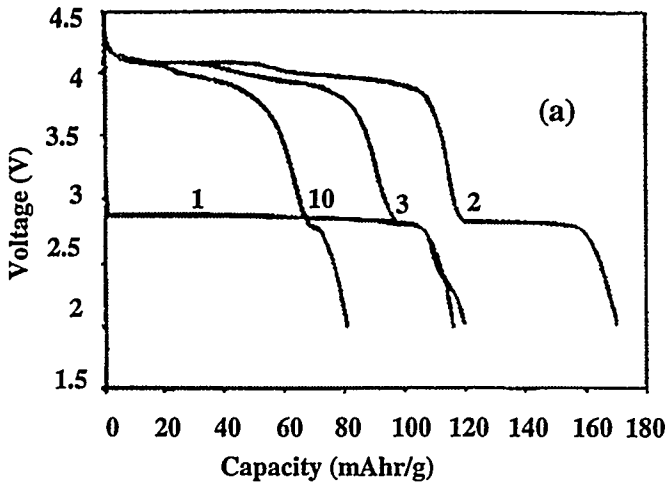
4.5
4
3.5
3
2.5
2
1.5
Voltage (V)
(a)
1
10
3
2
0 20 40 60 80 100 120 140 160 180
Capacity (mAhr/g)

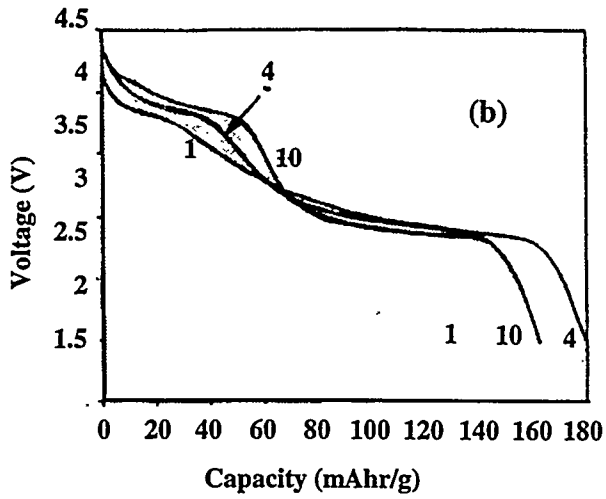
4.5
4
3.5
3
2.5
2
1.5
Voltage (V)
(b)
4
1
10
1 10 4
0 20 40 60 80 100 120 140 160 180
Capacity (mAhr/g)

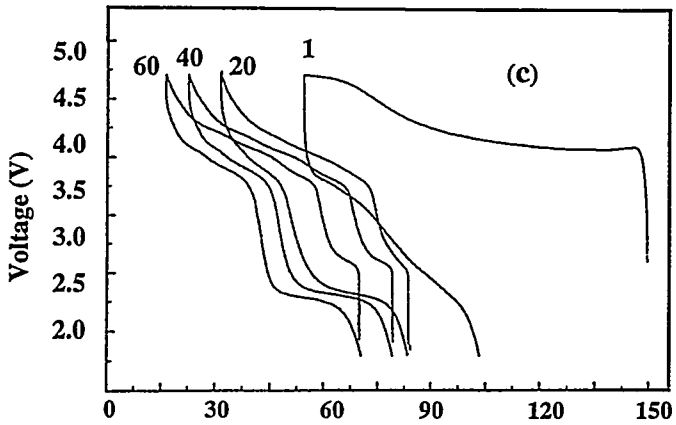
5.0
4.5
4.0
3.5
3.0
2.5
2.0
Voltage (V)
60
40
20
1
(c)
0 30 60 90 120 150

Fig. 1 (a-c)

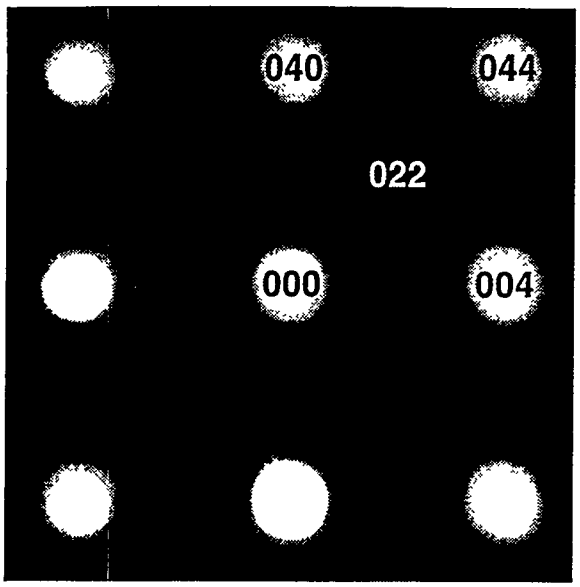

a)

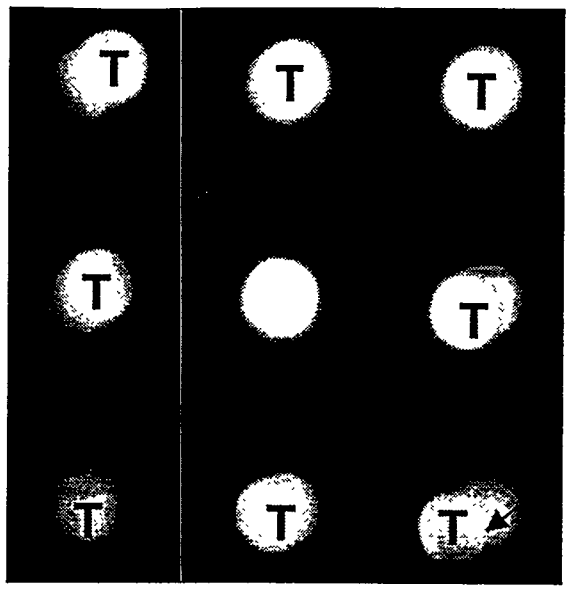

b)

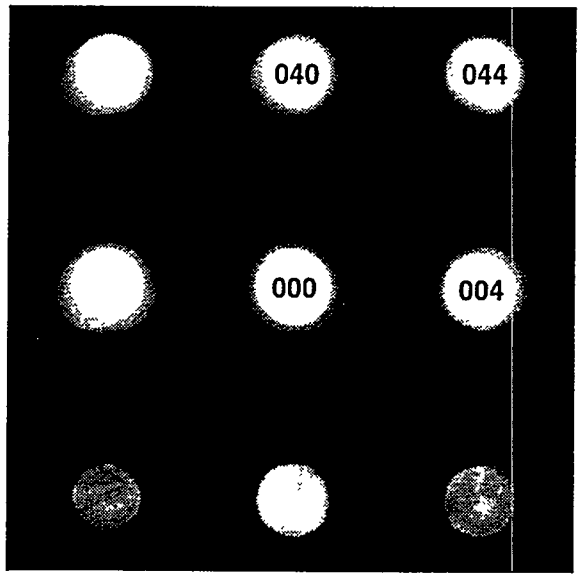

c)

Fig. 2 (a - c)

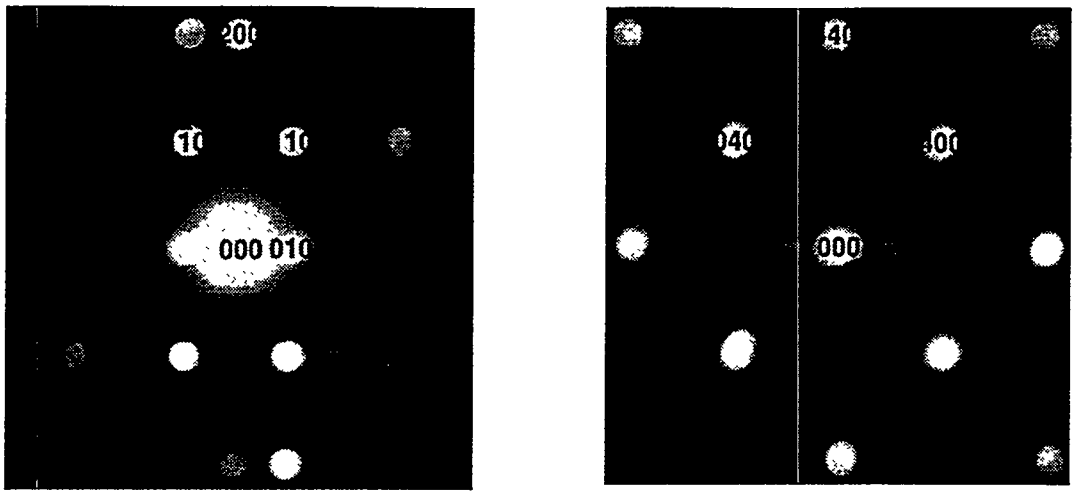

(a) (b)

Fig. 3 a, b

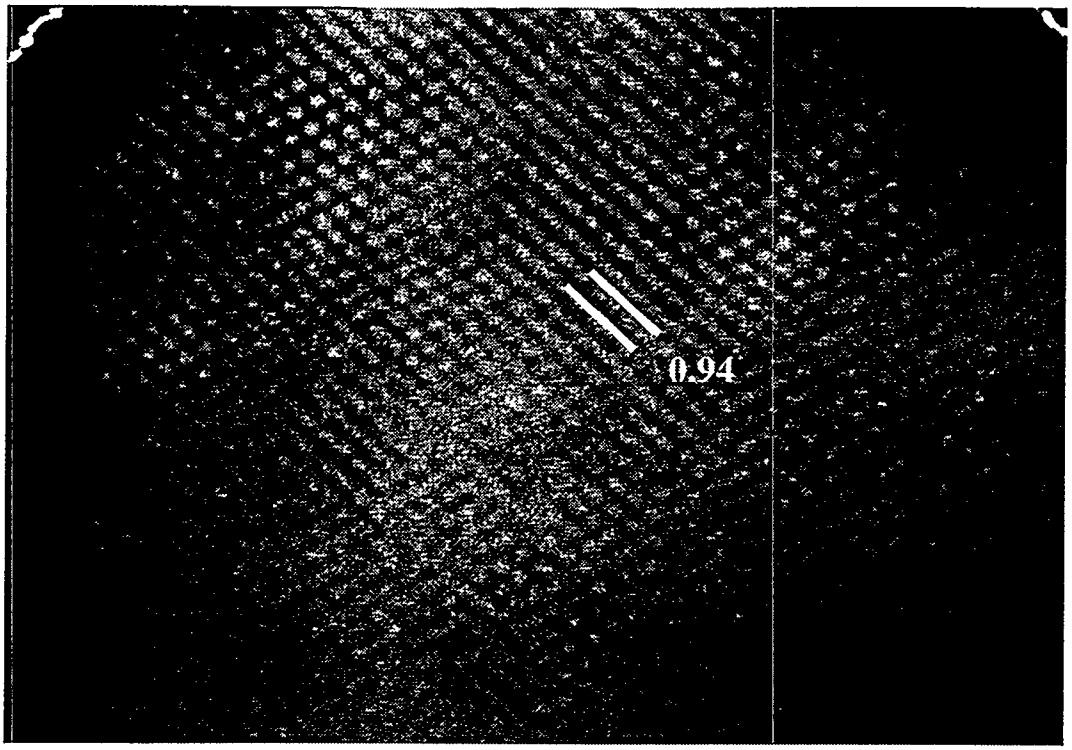

Fig. 4a

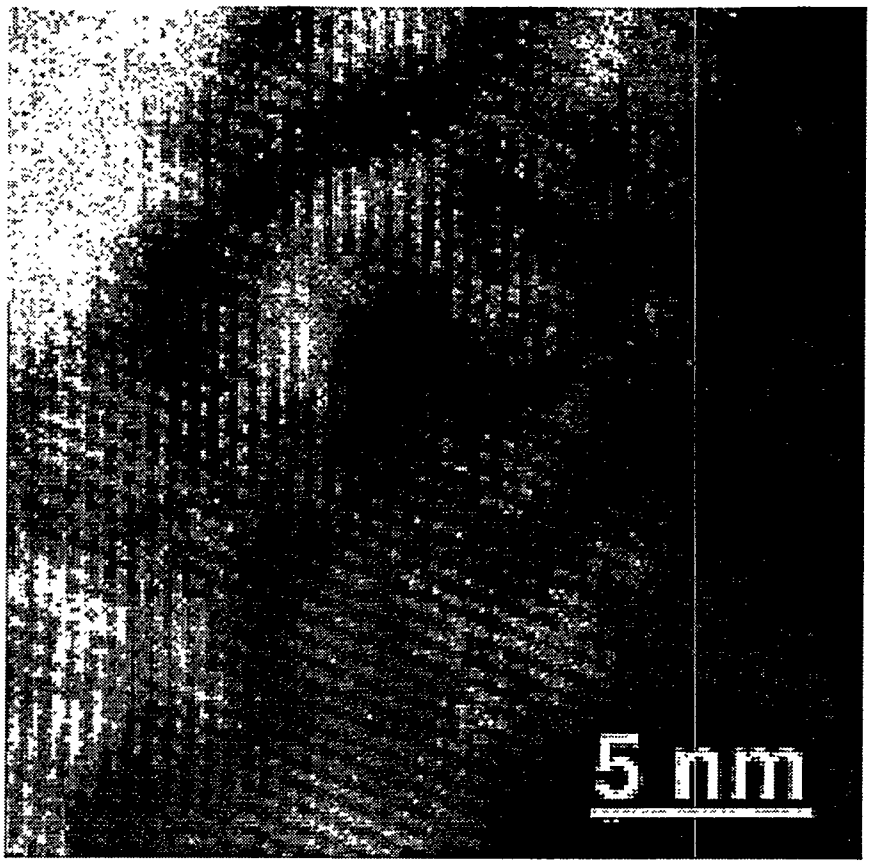

Fig. 4b

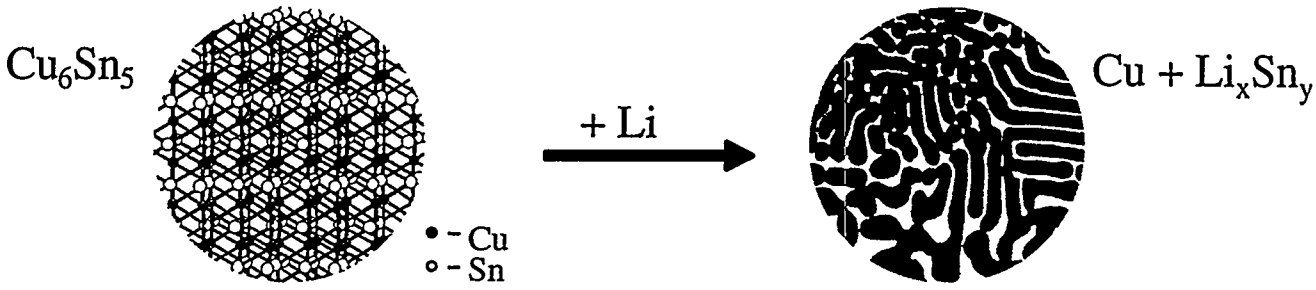

Fig. 5

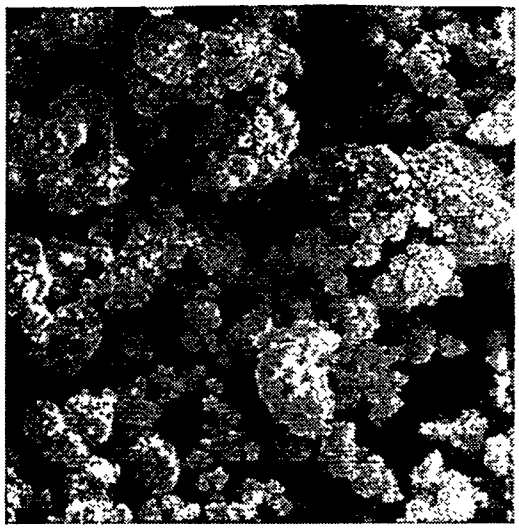

Sn L-line

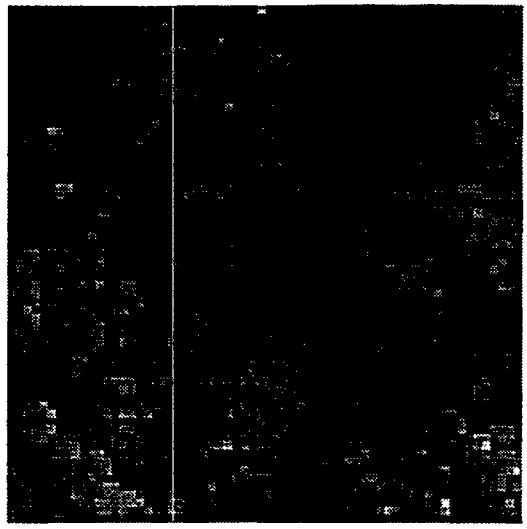

5 μm

Cu L-line

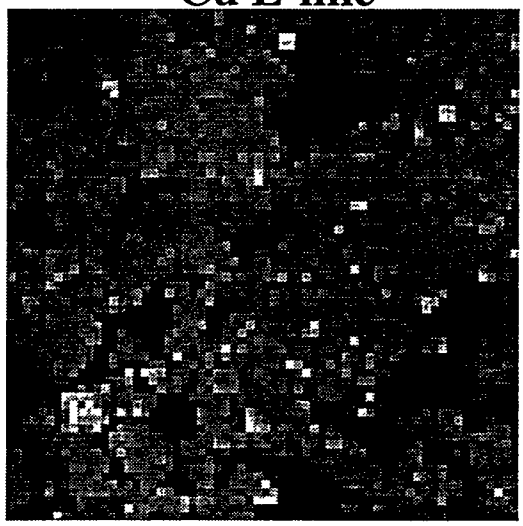

Fig. 6

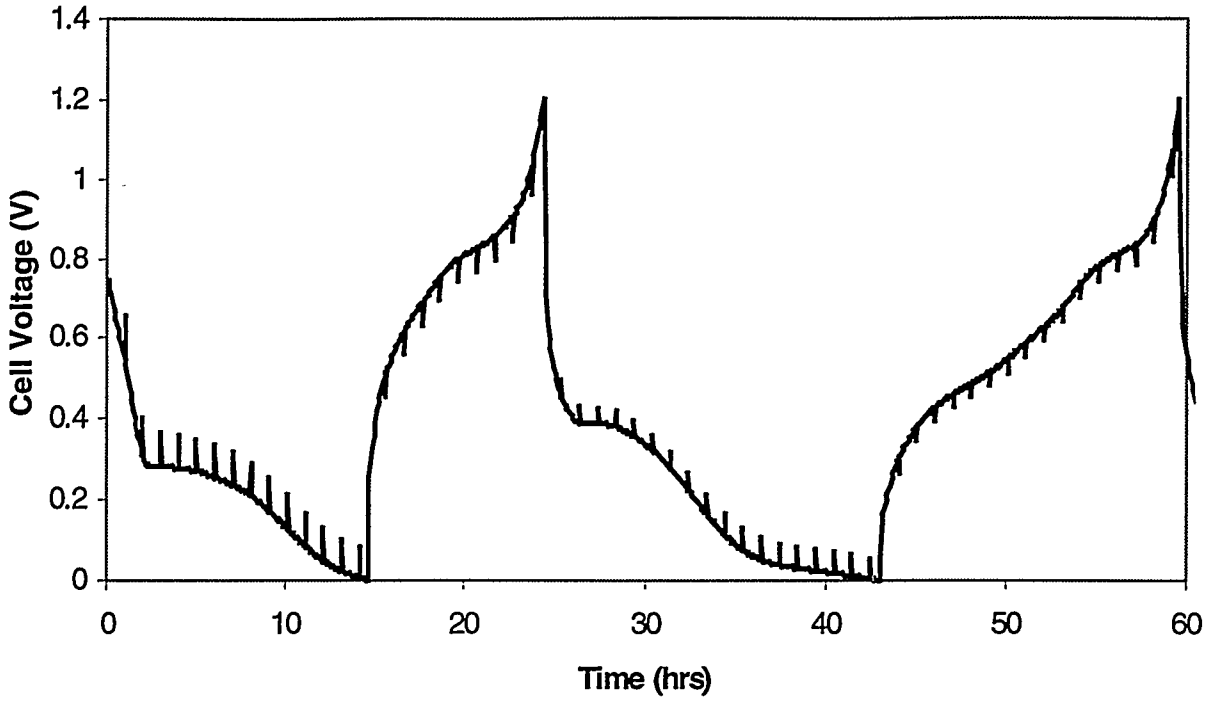

Fig. 7a

(Voltage range 1.2 to 0.2 V)